HHS Public Access

Author manuscript

J Chem Inf Model. Author manuscript; available in PMC 2023 April 11.

Published in final edited form as:

J Chem Inf Model. 2022 April 11; 62(7): 1760–1770. doi:10.1021/acs.jcim.1c01566.

The Hydrophobic/Hydrophilic Ratio of Amphiphilic Helix Mimetics Determines the Effects on Islet Amyloid Polypeptide Aggregation

Huayuan Tang[1], **Yunxiang Sun**[1,2], **Feng Ding**[1]

[1]Department of Physics and Astronomy, Clemson University, Clemson, SC 29634, United States

[2]Department of Physics, Ningbo University, Ningbo 315211, China

Abstract

Amyloid depositions of human islet amyloid polypeptide (hIAPP) are associated with type II diabetes (T2D) impacting millions of people globally. Accordingly, strategies against hIAPP aggregation are essential for the prevention and eventual treatment of the disease. Helix mimetics, which modulate the protein-protein interaction by mimicking the side chain residues of a natural α-helix, were found to be a promising strategy for inhibiting hIAPP aggregation. Here, we applied molecular dynamics simulations to investigate two helix mimetics reported to have opposite effects on hIAPP aggregation in solution – the oligopyridylamide-based scaffold **1e** promoted whereas naphthalimide-appended oligopyridylamide scaffold **DM 1** inhibited the aggregation of hIAPP in solution. We found that **1e** promoted the hIAPP aggregation due to the recruiting effects through binding with the N-termini of hIAPP peptides. In contrast, **DM 1** with a higher hydrophobic/hydrophilic ratio effectively inhibited hIAPP aggregation by strongly binding with the C-termini of hIAPP peptides, which competed for the inter-peptide contacts between amyloidogenic regions in the C-termini and impaired the fibrillization of hIAPP. Structural analyses revealed that **DM 1** formed the core of hIAPP-**DM 1** complexes and stabilized the off-pathway oligomers whereas **1e** formed the corona outside the hIAPP-**1e** complexes and remained active in recruiting free hIAPP peptides. The distinct interaction mechanisms of **DM 1** and **1e**, together with other reported potent antagonists in the literature, emphasized the effective small molecule-based amyloid inhibitors by disrupting peptide interactions should reach a balanced hydrophobic/hydrophilic ratio, providing a viable and generic strategy for the rational design of novel anti-amyloid nanomedicine.

Graphical Abstract

Corresponding Authors: Feng Ding, fding@clemson.edu;.

Author contributions

FD conceived the project. HT, YS and FD wrote the manuscript. HT, YS and FD performed DMD computer simulations and analysis. All authors agreed on the presentation of the manuscript.

Supplementary Material

The Supporting Information is available free of charge on the website. Secondary structure propensities of each hIAPP residue with hIAPP:**1e**/**DM 1**=4:4 (Figure S1); Histograms of hydrogen bonds and π-π stackings between helix mimetics and hIAPP peptides (Figure S2); Secondary structure propensities of each hIAPP residue with hIAPP: **DM 1**=5:1 (Figure S3). Residue-wise intra- and inter-peptide contact frequency map of hIAPP pentamer (Figure S4). Chemical structure of various amyloid inhibitors (Figure S5).

Conflict of Interest

The authors declare no conflict of interest.

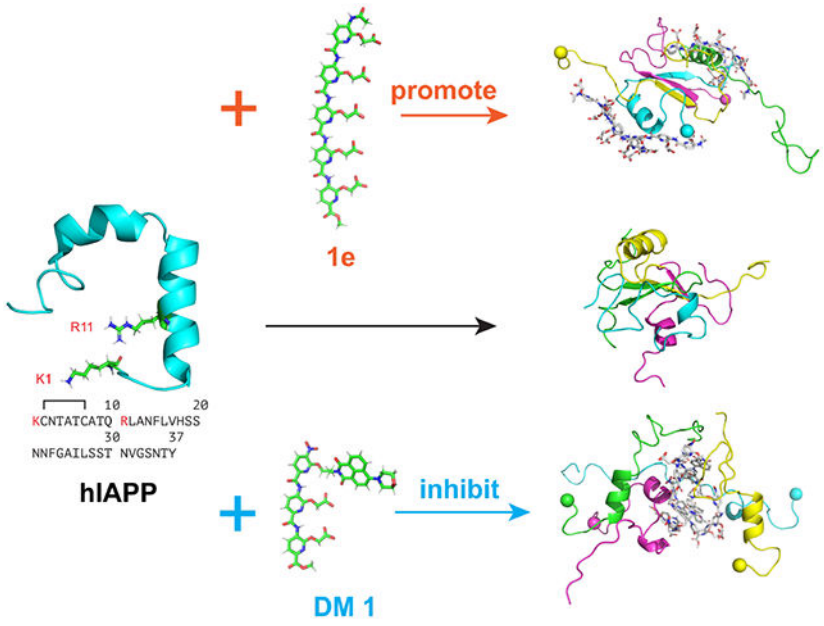

The effects of helix mimetics on human islet amyloid polypeptide aggregation depend on the hydrophobic/hydrophilic ratio

INTRODUCTION

The aberrant self-assemblies of proteins into amyloid fibrils with the generation of toxic intermediates along the process are hallmarks of multiple pathological disorders including Alzheimer's and Parkinson's diseases, and type II diabetes (T2D).[1,2] These insoluble β-sheet rich assemblies are formed via a series of conformational changes out of soluble, functional proteins. For instance, islet amyloid polypeptide (hIAPP) is the main component of amyloid deposits observed in the pancreatic islets of T2D patients and the amyloidogenesis process is linked to pancreatic inflammation, β-cell degeneration, and the pathogenesis of T2D.[3–5] hIAPP is a 37-residue hormone synthesized and stored in pancreatic β-cell islets, playing both functional roles as a neuropeptide regulator of glucose homeostasis and pathological role in the development and morbidity of T2D.[6] Prior to secretion, hIAPP is stabilized within intracellular β-cell granules by a combination of low pH and interactions with other granule components, including insulin, zinc ions and C-peptide.[7] However, under conditions of T2D, the intrinsically disordered but highly amyloidogenic hIAPP self-assembles into cytotoxic oligomers and amyloid fibrils within extracellular space, which eventually leads to dysfunction and death of β-cells in the pancreas.[8–10] Although the nature of toxic hIAPP species and the mechanisms of death of β-cells remain undetermined, mounting evidence supports one possible mechanism that the toxicity of hIAPP is rendered through its oligomerization along with structural transformations from disordered monomers to α-helical intermediates and then β-sheet-rich oligomers.[11,12] Subsequently, the oligomers can trigger a series of cellular responses including reactive oxygen species production, autophagy, apoptosis and extracellular matrix metabolism, which ultimately lead to β-cell death.

Numerous approaches have been explored to develop antagonists of hIAPP aggregation. Common strategies against hIAPP aggregation and toxicity often involve small molecules (e.g., biomimetics, curcumin, resveratrol, epigallocatechin gallate, dopamine, norepinephrine, etc.)[13–18], chaperone proteins (e.g., heat-shock protein 70, serum albumin, casein, etc.)[19] and nanoparticles (e.g., hydroxylated carbon-nanotube, fullerene, graphene, gold nanoparticles, dendrimers, star polymers, molybdenum disulfide, etc.)[20–26], and peptide-based inhibitors (e.g., hIAPP amyloid core derived d-peptide, etc.)[27]. The motivations are to interfere the amyloid aggregation through competing the amyloid peptide interactions by establishing hydrogen bond, hydrophobic interaction and π-stacking between the amyloid peptides and inhibitors, as the mechanisms revealed by molecular dynamics simulations.[16–18,23–27] Among them, helix mimetic is an appealing small molecular strategy for the inhibition of amyloid aggregation.[28–35] The basic idea of helix mimetics is to reproduce the side chain at residues *i*, *i*+3/*i*+4, and *i*+7 of a natural α-helix and modulate protein–protein interactions.[31] A library of helix mimetics has been synthesized and applied to inhibit protein aggregation, including hIAPP[32,33], Alzheimer's disease-related amyloid-β (Aβ) protein[34,35], and cancer-associated mutant p53 protein[30]. Intriguingly, the performances of these helix mimetics varied remarkably depending on the detailed molecular structures. Specifically, oligopyridylamide scaffold with five carboxy-terminated side chains to achieve the potential size and charge complementarity with the helical region of hIAPP region (**1e,** Figure 1A) were found to be able to inhibit hIAPP aggregation in the lipid environment but become effective aggregation agonists in the absence of lipid membranes.[33] In contrast, by appending an additional naphthalimide on an oligopyridylamide scaffold along with three carboxylate functionalities for targeting hydrophobic and cationic residues on hIAPP, **DM 1** was identified to be one of the most potent antagonists of hIAPP fibrillization both in the presence and absence of lipids, which can suppress the aggregation of hIAPP at a substoichiometric dose.[32] The above experimental results posed an intriguing question of why two helix mimetics **DM 1** and **1e** synthesized with size and charge complementary to hIAPP exhibited contrasting effects in modulating hIAPP aggregation in solution, and which properties should helix mimetics possess to be an effective inhibitor against hIAPP aggregation.

In this study, we applied atomistic discrete molecular dynamics (DMD) simulations to uncover the mechanism of action of **DM 1** and **1e** with contrasting modulating effects on hIAPP aggregation and determine the physicochemical determinant for efficient inhibition of amyloid aggregation. DMD is a rapid and predictive molecular dynamics algorithm, which has been used by many groups to study amyloid aggregation.[26,36,37] The analyses of aggregation kinetics, secondary structures and oligomer conformations of hIAPP in DMD simulations demonstrated that **DM 1** inhibited the aggregation of hIAPP whereas **1e** promoted the aggregation, consistent with the experimental observations. For **DM 1** with an additional hydrophobic portion, the naphthalimide-mediated hydrophobic interaction and π-π stackings enabled it to bind strongly with the C-terminal region of hIAPPs including the primary amyloidogenic core[11,38] (i.e., residues 22–29), which competed for the inter-peptide contacts and inhibited the hIAPP aggregation. The charged **1e** preferred to bind the N-termini of hIAPPs and were able to recruit multiple hIAPP peptides, promoting the fibrillization of hIAPPs by increasing the local concentration of peptides. In addition,

DM 1 stabilized the off-pathway oligomers by constituting the core of the hIAPP-**DM 1** complexes, whereas **1e** formed the corona outside the hIAPP-**1e** complexes and remained active in recruiting free hIAPP peptides. Thus, the opposite effects of **1e** and **DM 1** on hIAPP aggregation stressed the importance for helix mimetics to reach a balance between hydrophobic and hydrophilic components, which were further supported by existing amyloid antagonists[39,40], including recent helix mimetics with strong anti-amyloid properties[35]. Taken together, this study revealed the crucial role of hydrophobic/hydrophilic ratio in addition to size and charge complementary in inhibiting the amyloid aggregation by helix mimetics and offered rational design strategy of new helix mimetics-based nanomedicine.

MODELS AND METHODS

Discrete molecular dynamics simulations.

Computer simulations were performed with the united-atom discrete molecular dynamics (DMD). The continuous interaction potentials in classic molecular dynamics were replaced by discrete stepwise functions in DMD.[41] Collisions occurred when two atoms met at an energy step and their velocities were updated according to conservation laws. Thus, the system's dynamics in DMD was dictated by iteratively updating only the two colliding atoms, predicting their new collisions with corresponding neighbours, and finding the next collision via quick sort algorithms. Compared with classic molecular dynamics, the sampling efficiency of DMD is significantly enhanced and has been used by us and others to study protein folding, amyloid aggregation, and interactions with nanoparticles.[26,36,37] Interatomic interactions including bonded interactions (i.e., covalent bonds, bond angles, and dihedrals) and non-bonded interactions (i.e., van der Waals, solvation, hydrogen bond, and electrostatic terms) in our all-atom DMD simulations were adapted from the Medusa force field, which was benchmarked for accurate prediction of protein stability change upon mutation and protein–ligand binding affinity.[42,43]3/4/22 2:09:00 PM The force field parameters for van der Waals, covalent bonds, bond angles, and dihedrals were taken from CHARMM 19 force field.[44] Solvation was implicitly modelled by the effective energy function proposed by Lazaridis and Karplus.[45] The distance- and angle-dependent hydrogen bond interactions were modelled by a reaction-like algorithm.[46] The screened electrostatic interactions were computed using the Debye–Huckel approximation with the Debye length set to 10 Å, corresponding to a monovalent salt concentration of 100 mM.

Helix mimetics were modelled in all-atom DMD simulations using the MedusaScore, an extension of the Medusa force field.[43] The MedusaScore is consisted of the same weighted energy contributions as the Medusa force field (i.e., van der Waals (VDW), solvation, and hydrogen bonding energies) and has been parameterized using a large set of small molecule ligands.[43] The predictive power of the MedusaScore was validated in various benchmark studies, including accurate prediction of near-native ligand-binding poses and binding affinities during the prediction exercises of blind ligand-receptor docking organized by community structure-activity resource (CSAR).[47] Since the atom types and parameters are assigned in a consistent way as the original Medusa force field, the MedusaScore for small molecules is compatible with the protein simulations.[43,48,49] Combined with DMD, the force field has been shown to be able to accurately describe the interactions

between proteins and a wide variety of small molecules, including curcumin, resveratrol[50], epigallocatechin gallate (EGCG)[51], naringin[52], dendrimer[21], etc.

The initial structures of **DM 1** and **1e** were constructed by Avogadro.[53] Conformation of hIAPP monomer was taken from protein databank (PDB ID: 2L86). For each system, 39 independent simulations with different initial configurations and velocities were performed at 300 K, each of which lasted 650 ns with an accumulative simulation time of ~25 μs. A cubic box with periodic boundary conditions in three directions was used. For the systems with equimolar concentration of peptides and helix mimetics, four hIAPP peptides and four helix mimetics were simulated in a cubic box with dimension of 8.9 nm. For the systems with sub-stoichiometric concentration of helix mimetics, five hIAPP peptides with one helix mimetics were considered in a cubic box with dimension of 9.5 nm to maintain the same concentration of peptides at 4 mM.

Computational analysis.

The peptide secondary structure was calculated using the dictionary secondary structure of protein (DSSP) program.[54] A hydrogen bond was considered to be formed if the distance between the backbone N and O atoms within 3.5 Å and the angle of NH···O was larger than 120°. Residue-residue and residue-**1e**/**DM 1** contact were defined if they had at least one heavy atom contact within the cutoff distance of 0.65 nm. The π-π stackings between helix mimetics and residues with aromatic side chains were determined if the number of atomic contacts between aromatic rings was larger than 5.The radial distribution function $g(r)$ of atom in helix mimetics-hIAPP complexes with respect to the center of mass was calculated by $g(r) = N(r, r + \mathrm{d}r)/4\pi r^2 \mathrm{d}r$, where $N(r, r + \mathrm{d}r)$ was the number of atoms within the spherical shell with radii r and $r + \mathrm{d}r$ measured from the center of the complex. Two-dimensional potential of mean force (PMF) was obtained via the probability distribution, i.e., $-k_B T \log P(n_{\mathrm{oligomer}}, e_{\beta-\mathrm{sheet}})$, where $P(n_{\mathrm{oligomer}}, e_{\beta-\mathrm{sheet}}$ was the probability of conformations with oligomer size n_{oligomer} and β-sheet content $e_{\beta-\mathrm{sheet}}$

RESULTS AND DISCUSSION

hIAPP self-assembly in the presence and absence of two helix mimetics

Aggregations of four hIAPP peptides with and without an equimolar of **1e**/**DM 1** were simulated in DMD simulations. For each of the three molecular systems, about forty independent simulations were performed starting from different initial configurations with randomized velocities and inter-molecular distances and orientations (Methods). Averaged over independent simulations, time evolutions of the mass-weighted cluster size and β-sheet content of hIAPP peptides in the absence and presence of helix mimetics were shown in Figures 1B&C. In the absence of helix mimetics, hIAPP peptides aggregated into large oligomers within 100 ns, after which the average oligomer size fluctuated around 3.4, suggesting the dynamic binding and unbinding of peptides. In the presence of helix mimetics, the hIAPP peptides can aggregate into larger oligomers in a shorter time, indicating the effective binding of both **DM 1** and **1e** with the peptides. After binding with hIAPP peptides, **DM 1** facilitated the formation of stable tetramers with the population higher than 97%, whereas the hIAPP oligomers formed with **1e** remained dynamic with

averaged size larger than control (Figures 1B&S1). At the initial aggregation stage, the β-sheet content of hIAPP peptides in the presence of **1e** remained almost the same as that of the control group with peptides alone. After reaching steady states, the β-sheet content of hIAPP peptides with **1e** raised to a higher level than the control group, consistent with the promotion effects of **1e** on hIAPP aggregation observed in experiments. The effects of **1e** in reducing the lag time of hIAPP self-assembly and β-sheet formation were subtle in simulations (the relaxation time τ obtained by fitting the time evolution of β-sheet content were ~27.39 ns for hIAPP alone and ~27.70 ns for hIAPP:**1e**=4:4, see the fitted lines in Figure 1C) due to the fast aggregation kinetics under high peptide concentration *in silico* (~ 4 mM) than the experimental condition (usually at μM range). In contrast, the β-sheet content of hIAPP peptides with the presence of **DM 1** reduced to a lower level with a longer lag time compared to hIAPP peptides alone (the relaxation time was ~30.5 ns for hIAPP:**DM 1**=4:4, see Figure 1C), which were consistent with the experiments.[32] Hence, kinetics analyses of simulation trajectories showed that **DM 1** inhibited the hIAPP aggregation by retarding the lag time and reducing the β-sheet structure content, whereas **1e** promoted the hIAPP aggregation by elevating the β-sheet structure in steady state with effects on the aggregation lag time potentially shadowed by the high peptide concentration used in simulations.

The effect of helix mimetics on the aggregation kinetics of hIAPP were further analyzed by calculating the two-dimensional potential of mean force (PMF) with respect to the oligomer size and β-sheet content (Figure 2). The PMFs featured two basins with the first basin (i.e., i, I, and i') corresponding to the monomeric state with a low β-sheet content and the second basin (i.e., ii, II, and ii') corresponding to the tetramers with a relatively high β-sheet content. In the presence of **1e**, the basin of oligomers (basin II) with a relatively high β-sheet content became broader (Figure 2B). Moreover, the energy barrier for the oligomer nucleation (ΔE_1) was reduced (ΔE_1=0.81 k_BT for hIAPP alone and ΔE_1=0.72 k_BT for hIAPP:**1e**=4:4) and the tetramer state became more stable compared to the monomeric state with lower free energy (ΔE_2=−1.35 k_BT for hIAPP alone and ΔE_2=−1.66 k_BT for hIAPP:**1e**=4:4) (Figures 2D&E), which suggested that **1e** facilitated the transformation of hIAPP from monomeric state to oligomeric state with a high β-sheet content. In contrast, the free energy basin in oligomeric state (basin i') featured low β-sheet content in the presence of **DM 1** (Figure 2C). At the same time, the oligomeric state became more energetically favorable compared to the control (ΔE_2=−3.53 k_BT) with the energy barrier for nucleation kept almost unchanged (ΔE_1=0.80 k_BT) (Figure 2D&E), which meant that **DM 1** favored the formation of hIAPP oligomers with low β-sheet structures. Therefore, the free energy landscape analyses revealed that **1e** facilitated the formation of oligomers with high β-sheet contents whereas **DM 1** rendered the formation of oligomers with low b-sheet contents.

The secondary structure propensities of each hIAPP residue after the simulations reached steady states were also analyzed to evaluate the detailed secondary structure changes of hIAPP induced by helix mimetics, (Figures 3&S1). In the absence of helix mimetics, the N-terminus of hIAPP, especially A8-F15, had a high propensity to form a helical structure, which was consistent with site-specific two-dimensional IR spectroscopy and NMR results[55,56]. Obvious β-sheet structure can be observed at residues 16–20 and 25–

29, which also agreed well with previous studies[57]. In the presence of an equimolar concentration of **1e**, the β-sheet structure of residues 3–31 increased due to the unfolding of helix structures (Figures 3A&B). In comparison, **DM 1** increased the helix propensity of residues 18–26 and significantly decreased the propensity of β-sheet structure at residues 16–21 and 25–32 (Figures 3C&D). As a result, **1e** reduced the overall helix propensity and increased the β-sheet propensity of hIAPP peptides, whereas **DM 1** enhanced the overall helix propensity and decreased the β-sheet propensity (Figure 3E). For both **1e** and **DM 1**, the coil and bend structure propensity remained almost unchanged and the turn propensity slightly reduced (Figures 3E&S1).

Differential binding of DM 1 and 1e with hIAPP peptides

To elucidate the molecular mechanism for the opposite effects of **DM 1** and **1e** on the hIAPP aggregation, binding frequencies of each hIAPP residue with **DM 1** and **1e** were calculated (Figure 4A). Due to the structural similarities, **DM 1** and **1e** possessed similar binding properties with the first 15 residues of hIAPP peptides, where the binding was dominated by the electrostatic interactions (K1 and R11) and π-π stackings (e.g., F15) (Figures 4B&C). The most intriguing feature is that the binding affinities between **DM 1** and hIAPP residues 16–37 including the amyloidogenic core sequence of 22–29[11,38]. were much higher than those with **1e**. The enhanced binding affinities between **DM 1** and hIAPP C-terminal region can be attributed to the hydrophobic interactions between the naphthalimide and hydrophobic residues (e.g., F23, I26, L27, Y37, etc.). Examination of typical snapshots of hIAPP-**DM 1** and hIAPP-**1e** complexes confirmed that the extensive hydrogen bonds and π-π stacking have been formed between the oligopyridylamide scaffold and the peptide backbones or side chains (Figures 4B&C), suggesting these characteristic interactions associated with the helix mimetics were essential for the hetero-molecular complex formation. For **DM 1**, the hydrogen bonding with hIAPP peptides and π-π stackings with the aromatic residues of the hIAPP were higher than these with **1e**, due to the appending of naphthalimide groups (Figures S2). The C-terminal residues of hIAPP, especially the amyloidogenic core of residues 22–29, strongly influenced and contributed towards hIAPP aggregation. The amyloidogenic regions of hIAPP peptides were found to play a crucial role in the peptide self-association and aggregation[11,38]. When these residues took part in hydrophobic interactions and π-π stackings with **DM 1**, inter-peptide interactions would be diminished and thus the aggregation was inhibited. Taken together, we found that **DM 1** showed higher binding affinities with the C-terminus of hIAPP than **1e** due to the hydrogen bond formation and π-π stackings with naphthalimide groups.

To further characterize the influences of **DM 1** and **1e** on the assemblies of hIAPP peptides, residue-wise intra- and inter-peptide contact frequency maps were calculated after the simulations reached steady states (Figure 5). For hIAPP tetramers in control simulations, the high intra-peptide contacts in the diagonal region of A8-F15 corresponded to the highly helical structure (Figure 3). Inter-peptide contacts were rich between 16–20 and 25–29, confirming the formation of β-sheet structure in these two regions. The presence of **1e** increased the overall inter-chain contacts with a noticeable enhancement of inter-peptide contacts between the amyloidogenic core of hIAPP (residues 22–29) (Figure 5B). As a result, the β-sheet propensity of hIAPP residues, especially in the amyloidogenic region, was

promoted (Figure 3B). The diagonal region of intra-peptide contacts decreased, indicating the unfolding of helix structures. Together with the binding affinities with **1e** (Figure 4A), the contact frequency maps suggested that **1e** recruited hIAPPs via electrostatic interactions with the N-termini, subsequently increasing the local hIAPP concentration and enhancing inter-peptide interactions between the amyloidogenic regions near the hIAPP C-termini to promote hIAPP fibrillization. In contrast, **DM 1** suppressed the inter-peptide contacts between the residues 16–20 and 25–29 despite the increased inter-peptide contacts in the other regions due to the recruiting effect of **DM 1** (Figure 5C). In addition, the enhanced intra-peptide contacts in the diagonal region of 16–20 and 25–29 suggested **DM 1** can stabilize the helix structure, the unfolding of which were crucial for the fibrillization of hIAPP. Therefore, **DM 1** inhibited the hIAPP fibrillization by reducing the inter-peptide contacts between amyloidogenic region and stabilizing the helix structure.

Distinct 3D structures of hIAPP-DM 1 and hIAPP-1e complexes

To further reveal the structural characteristics of the hIAPP-**DM 1** and hIAPP-**1e** complexes, we calculated the radial distribution functions of peptide atoms and small molecular atoms as a function of the distance measured from the center of mass of the complexes, averaged over the structural ensemble of corresponding oligomers (Figure 6). The peak density of **1e** atoms occurred at a larger distance than that of hIAPP peptide atoms in hIAPP-**1e** complexes, whereas the peak density of **DM 1** atoms occurred at a shorter distance than that of hIAPP peptide atoms in hIAPP-**DM 1** complexes (Figures 6A&B). Thus, **1e** positioned outside of the complexes and formed the corona of the hIAPP oligomers, whereas **DM 1** located inside the complexes and instead formed the core of oligomers. The contrast positioning of **DM 1** and **1e** with respect to hIAPP peptides in the complexes were confirmed by the representative snapshots (Figures 6C&D). In addition, the exposed **1e** in hIAPP-**1e** complexes were able to recruit additional hIAPP peptides from the solution, which can further promote the hIAPP fibrillization. In contrast, the C-terminal regions of hIAPP tended to be buried in the core of oligomer due to its high binding affinity with **DM 1**, which were similar with the structures of small-weight hIAPP oligomers formed with polyphenols including curcumin and resveratrol[50]. In these cases, the buried amyloidogenic regions were prevented from further interactions with other peptides, thus stabilizing the off-pathway oligomers.

DM 1 inhibits hIAPP aggregation substoichiometrically

The above discussions showed that the naphthalimide group enabled **DM 1** to suppress the aggregation of hIAPP at equimolar concentrations. One appealing properties of **DM 1** was that it remained functional at substoichiometric concentrations compared to the high dose requirements for other small molecular inhibitors.[58] Here, we also performed DMD simulations of five hIAPP and one **DM 1** in accordance with experimental results that 0.2 equivalents of **DM 1** were effective in suppressing hIAPP aggregation.[32]

Figures 7A&B showed at the substoichiometric concentration, **DM 1** remained effective in stabilizing α-helical structure and reducing the β-sheet structure propensities at residues 16–21 and 25–32 with the extent much slighter than those with equimolar **DM 1** (Figures 3&S3). The overall secondary structure contents also suggested the noticeable enhancement

of α-helical structure and reduction of the β-sheet structure of hIAPP peptides in the presence of 0.2 equivalents of **DM 1** (Figure 7C). Similar with the equimolar concentration cases, both the inter- and intra-peptide contacts between amyloidogenic regions of hIAPP peptides were reduced by 0.2 equivalents of **DM 1** (Figures 7D, E&S4), indicating that the inhibition mechanisms described above remained valid. On average, one **DM 1** molecule can bind with at least three hIAPP peptides to interfere inter-peptide contacts in more than 95% of the total conformation ensembles (Figure 7F), explaining the ability of **DM 1** to function at substoichiometric doses. Furthermore, the single **DM 1** molecule positioned in the center of hIAPP-**DM 1** complex to stabilize the off-pathway oligomers, as illustrated by the typical conformations (Figure 7G). Collectively, our simulations confirmed that **DM 1** was able to inhibit hIAPP aggregation substoichiometrically.

The hydrophobic-to-hydrophilic ratio of helix mimetics and the anti-aggregation functions

A major structural difference of **DM 1** with respect to **1e** is the hydrophobic naphthalimide group appended on the oligopyridylamide scaffold, which makes **DM 1** essentially with a higher hydrophobic/hydrophilic ratio. The molecular structures suggested that the effective helix mimetics-based amyloid inhibitors should reach a delicate balance of the hydrophobic-to-hydrophilic ratio. The notion is supported by that various **DM 1** variants showed no or less effect on hIAPP aggregation.[32] Specifically, hydrophilic bispyridylamide **DM 2** and trispyridylamide **DM 3**, having two and three acidic groups respectively without the hydrophobic naphthalimide group (Figure S5A), did not affect hIAPP aggregation. On the other hand, simple hydrophobic monopyridyl **DM 5** and carboxylated naphthalimide **DM 6** also had no effect on hIAPP aggregation (Figure S5A). In addition, bispyridylamide **DM 4**, containing a naphthalimide and a carboxylate group (Figure S5A) which was less hydrophilic than **DM 1**, delayed hIAPP aggregation with a lesser extent. In addition, the more recently developed helix mimetics ADH-353 (Figure S5B), which contained one hydrophobic N-butyl and two hydrophilic N-propylamine side chains, attenuated cytotoxicity by inhibiting Aβ fibrillization in a strict molecular structure-dependent way. Small deviations from the optimal hydrophilic/hydrophobic arrangement resulted in the loss of inhibitory effects.[35] The increase of hydrophobic/hydrophilic ratio of helix mimetics led the assembles of inhibitors varying from isolate monomer to micelles and vesicles. Consistent with this notion, **1e** did not self-assemble in our simulations (Figure 6C), while **DM 1** assembled into a small micelle-like core in the center of hIAPP-**DM 1** complexes (Figure 6D) and ADH-353 with larger hydrophobic portions formed stable vesicles under physiological conditions. The micelles or vesicles with localized inhibitor concentrations provided multiple binding sites for the amyloid peptides, thus effectively inhibited their aggregations. Taken together, these findings support that effective helix mimetics-based inhibitors should reach a delicate balance between hydrophobic and hydrophilic components.

Besides helix mimetics, many reported amyloid inhibitors in the literature also featured a delicately balanced hydrophobic-to-hydrophilic ratio. Fullerenols with intermediated hydrophobic/hydrophilic ratios exhibited significant inhibition effects on the amyloid aggregation of alpha-synuclein NACore, while highly hydrophobic or hydrophilic fullerenols had no or weak effects.[39] Amphiphilic compound LS-4, consisting of a

hydrophobic amyloid fibril-binding fragment and a hydrophilic azamacrocycle (Figure S5C), exhibited dramatically enhanced binding affinity toward various Aβ aggregate species compared to the compound Pre-LS-4, which contained only the hydrophobic conjugated aromatic fragment (Figure S5C)[40]. As a negative control, heparin, the highly sulphated linear polysaccharide, promoted the aggregations of hIAPP, Aβ, alpha-synuclein and β2-microglobulin, similar to the negatively charged **1e**.[59–61] Taken together, our simulations and the above reports support the notion that a delicate balance between hydrophobicity and hydrophilicity is likely necessary for eliciting inhibition effects on amyloid aggregation. This can be understood by the fact that amyloid proteins and peptides are intrinsically amphiphilic polymers. Thus, the inhibitors with balanced hydrophobic/hydrophilic ratios maximize their disrupting effects on amyloid aggregations in dual ways, namely the hydrophobic components of inhibitors drive the binding with amyloidogenic peptides and polar groups of inhibitors compete with the formation of inter-peptide hydrogen bonds by forming hydrogen bonds with peptide backbones.

Conclusion

Human hIAPP forms amyloid deposits in the islets of Langerhans, a phenomenon associated with type-2 diabetes impacting millions of people worldwide. Accordingly, strategies against hIAPP aggregation are essential for the prevention and eventual treatment of the disease. Here, we investigated the molecular mechanism for the opposite modulating effect of two helix mimetics - amphiphilic **DM 1** and highly charged **1e** - on hIAPP aggregation via discrete molecular dynamics and explored the role of hydrophobic/hydrophilic ratio in the design of helix mimetics-based amyloid inhibitor. Consistent with experiments, **DM 1** was found to reduce the β-sheet structure propensity and stabilize the helix structure, whereas **1e** facilitated the conversion of helix structure into the β-sheet structure. The molecular mechanisms for the opposite effects of **DM 1** and **1e** were revealed by the different binding behaviors with hIAPP peptides. Specifically, the helix mimetic **DM 1** with a higher hydrophobic portion had a strong binding affinity with the C-termini of hIAPPs driven by the hydrogen bonding, hydrophobic interactions and **π-π** stacking interactions with the appended naphthalimide group of **DM 1**. Thus, **DM 1** competed for the inter-peptide contacts between C-termini of hIAPPs which were crucial for the fibrillization of hIAPP, resulting in effective prevention of hIAPP aggregation. However, in the absence of the hydrophobic naphthalimide group, **1e** bound with the N-termini of hIAPP peptides and effectively recruited hIAPPs via hydrophobic and electrostatic interactions with the N-termini, subsequently increasing the local hIAPP concentration and enhancing inter-peptides interactions between the amyloidogenic regions near the hIAPP C-termini to promote hIAPP fibrillization. Further structural analyses revealed that **DM 1** formed the core of hIAPP-**DM 1** complexes and stabilized the off-pathway oligomers, whereas **1e** formed the corona outside the hIAPP-**1e** complexes and remained active in recruiting free hIAPP peptides.

The distinct performances and interaction mechanisms of **DM 1** and **1e** with hIAPP peptides emphasized the pivotal roles of the balance between hydrophobic and hydrophilic components for helix mimetics, which enabled them to provide multiple binding sites in a concentrated volume by forming micelles or vesicles, to be effective hIAPP aggregation

inhibitors. The situation in the presence of lipids, where both **1e** and **DM 1** inhibited the aggregation of hIAPP, required further investigation in the future. The current study, together with reported potent antagonists and their variants, suggested that effective small molecule-based amyloid inhibitors that target at the amyloidogenic core regions and compete for the amyloid peptide interactions, should possess balanced hydrophobic/hydrophilic ratios, providing a facile strategy for the optimal design of new anti-amyloid medicines.

Supplementary Material

Refer to Web version on PubMed Central for supplementary material.

Acknowledgements

This work was supported by NSF CAREER CBET-1553945 (Ding) and NIH MIRA R35GM119691 (Ding). This work was also supported in part by the National Natural Science Foundation of China under the grant no. 11904189 (Y.S.)

Data and Software Availability

DMD simulation engine is available at Molecules In Action, LLC. (www.moleculesinaction.com). Input files, initial conformations for DMD simulations, and representative DMD trajectories for each system are available (https://dlab.clemson.edu/research/HelixMimetics/).

References:

(1). Selkoe DJ Folding Proteins in Fatal Ways. Nature 2003, 426, 900–904. [PubMed: 14685251]

(2). Chiti F; Dobson CM Protein Misfolding, Functional Amyloid, and Human Disease. Annu. Rev. Biochem 2006, 75, 333–366. [PubMed: 16756495]

(3). Morikawa S; Kaneko N; Okumura C; Taguchi H; Kurata M; Yamamoto T; Osawa H; Nakanishi A; Zako T; Masumoto J IAPP/Amylin Deposition, Which Is Correlated with Expressions of ASC and IL-1β in β-Cells of Langerhans' Islets, Directly Initiates NLRP3 Inflammasome Activation. Int. J. Immunopathol. Pharmacol 2018, 32, 205873841878874.

(4). Ying W; Fu W; Lee YS; Olefsky JM The Role of Macrophages in Obesity-Associated Islet Inflammation and β-Cell Abnormalities. Nat. Rev. Endocrinol 2020, 16, 81–90. [PubMed: 31836875]

(5). Milardi D; Gazit E; Radford SE; Xu Y; Gallardo RU; Caflisch A; Westermark GT; Westermark P; Rosa CL; Ramamoorthy A Proteostasis of Islet Amyloid Polypeptide: A Molecular Perspective of Risk Factors and Protective Strategies for Type II Diabetes. Chem. Rev 2021, 121, 1845–1893. [PubMed: 33427465]

(6). Akter R; Cao P; Noor H; Ridgway Z; Tu L-H; Wang H; Wong AG; Zhang X; Abedini A; Schmidt AM; Raleigh DP Islet Amyloid Polypeptide: Structure, Function, and Pathophysiology. J. Diabetes Res 2016, 2016, 1–18.

(7). Westermark P; Li Z-C; Westermark GT; Leckström A; Steiner DF Effects of Beta Cell Granule Components on Human Islet Amyloid Polypeptide Fibril Formation. FEBS Lett. 1996, 379, 203–206. [PubMed: 8603689]

(8). Cao Q; Boyer DR; Sawaya MR; Ge P; Eisenberg DS Cryo-EM Structure and Inhibitor Design of Human IAPP (Amylin) Fibrils. Nat. Struct. Mol. Biol 2020, 27, 653–659. [PubMed: 32541896]

(9). Röder C; Kupreichyk T; Gremer L; Schäfer LU; Pothula KR; Ravelli RBG; Willbold D; Hoyer W; Schröder GF Cryo-EM Structure of Islet Amyloid Polypeptide Fibrils Reveals Similarities with Amyloid-β Fibrils. Nat. Struct. Mol. Biol 2020, 27, 660–667. [PubMed: 32541895]

(10). Gallardo R; Iadanza MG; Xu Y; Heath GR; Foster R; Radford SE; Ranson NA Fibril Structures of Diabetes-Related Amylin Variants Reveal a Basis for Surface-Templated Assembly. Nat. Struct. Mol. Biol 2020, 27, 1048–1056. [PubMed: 32929282]

(11). Buchanan LE; Dunkelberger EB; Tran HQ; Cheng P-N; Chiu C-C; Cao P; Raleigh DP; de Pablo JJ; Nowick JS; Zanni MT Mechanism of IAPP Amyloid Fibril Formation Involves an Intermediate with a Transient -Sheet. Proc. Natl. Acad. Sci 2013, 110, 19285–19290. [PubMed: 24218609]

(12). Nguyen PH; Ramamoorthy A; Sahoo BR; Zheng J; Faller P; Straub JE; Dominguez L; Shea J-E; Dokholyan NV; De Simone A; Ma B; Nussinov R; Najafi S; Ngo ST; Loquet A; Chiricotto M; Ganguly P; McCarty J; Li MS; Hall C; Wang Y; Miller Y; Melchionna S; Habenstein B; Timr S; Chen J; Hnath B; Strodel B; Kayed R; Lesné S; Wei G; Sterpone F; Doig AJ; Derreumaux P Amyloid Oligomers: A Joint Experimental/Computational Perspective on Alzheimer's Disease, Parkinson's Disease, Type II Diabetes, and Amyotrophic Lateral Sclerosis. Chem. Rev 2021, 121, 2545–2647. [PubMed: 33543942]

(13). Yan L-M; Tatarek-Nossol M; Velkova A; Kazantzis A; Kapurniotu A Design of a Mimic of Nonamyloidogenic and Bioactive Human Islet Amyloid Polypeptide (IAPP) as Nanomolar Affinity Inhibitor of IAPP Cytotoxic Fibrillogenesis. Proc. Natl. Acad. Sci 2006, 103, 2046–2051. [PubMed: 16467158]

(14). Abedini A; Meng F; Raleigh DP A Single-Point Mutation Converts the Highly Amyloidogenic Human Islet Amyloid Polypeptide into a Potent Fibrillization Inhibitor. J. Am. Chem. Soc 2007, 129, 11300–11301. [PubMed: 17722920]

(15). Meng F; Abedini A; Plesner A; Verchere CB; Raleigh DP The Flavanol (−)-Epigallocatechin 3-Gallate Inhibits Amyloid Formation by Islet Amyloid Polypeptide, Disaggregates Amyloid Fibrils, and Protects Cultured Cells against IAPP-Induced Toxicity. Biochemistry 2010, 49, 8127–8133. [PubMed: 20707388]

(16). Mo Y; Lei J; Sun Y; Zhang Q; Wei G Conformational Ensemble of HIAPP Dimer: Insight into the Molecular Mechanism by Which a Green Tea Extract Inhibits HIAPP Aggregation. Sci. Rep 2016, 6, 33076. [PubMed: 27620620]

(17). Lao Z; Chen Y; Tang Y; Wei G Molecular Dynamics Simulations Reveal the Inhibitory Mechanism of Dopamine against Human Islet Amyloid Polypeptide (HIAPP) Aggregation and Its Destabilization Effect on HIAPP Protofibrils. ACS Chem. Neurosci 2019, 10, 4151–4159. [PubMed: 31436406]

(18). Roy R; Paul S Theoretical Investigation of the Inhibitory Mechanism of Norepinephrine on HIAPP Amyloid Aggregation and the Destabilization of Protofibrils. J. Phys. Chem. B 2020, 124, 10913–10929. [PubMed: 33207866]

(19). Thorn DC; Meehan S; Sunde M; Rekas A; Gras SL; MacPhee CE; Dobson CM; Wilson MR; Carver JA Amyloid Fibril Formation by Bovine Milk κ-Casein and Its Inhibition by the Molecular Chaperones α_S - and β-Casein. Biochemistry 2005, 44, 17027–17036. [PubMed: 16363816]

(20). Gladytz A; Abel B; Risselada HJ Gold-Induced Fibril Growth: The Mechanism of Surface-Facilitated Amyloid Aggregation. Angew. Chem. Int. Ed 2016, 55, 11242–11246.

(21). Gurzov EN; Wang B; Pilkington EH; Chen P; Kakinen A; Stanley WJ; Litwak SA; Hanssen EG; Davis TP; Ding F; Ke PC Inhibition of HIAPP Amyloid Aggregation and Pancreatic β-Cell Toxicity by OH-Terminated PAMAM Dendrimer. Small 2016, 12, 1615–1626. [PubMed: 26808649]

(22). Javed I; Sun Y; Adamcik J; Wang B; Kakinen A; Pilkington EH; Ding F; Mezzenga R; Davis TP; Ke PC Cofibrillization of Pathogenic and Functional Amyloid Proteins with Gold Nanoparticles against Amyloidogenesis. Biomacromolecules 2017, 18, 4316–4322. [PubMed: 29095600]

(23). Mo Y; Brahmachari S; Lei J; Gilead S; Tang Y; Gazit E; Wei G The Inhibitory Effect of Hydroxylated Carbon Nanotubes on the Aggregation of Human Islet Amyloid Polypeptide Revealed by a Combined Computational and Experimental Study. ACS Chem. Neurosci 2018, 9, 2741–2752. [PubMed: 29986579]

(24). Koppel K; Tang H; Javed I; Parsa M; Mortimer M; Davis TP; Lin S; Chaffee AL; Ding F; Ke PC Elevated Amyloidoses of Human IAPP and Amyloid Beta by Lipopolysaccharide and Their Mitigation by Carbon Quantum Dots. Nanoscale 2020, 12, 12317–12328. [PubMed: 32490863]

(25). Bai C; Lao Z; Chen Y; Tang Y; Wei G Pristine and Hydroxylated Fullerenes Prevent the Aggregation of Human Islet Amyloid Polypeptide and Display Different Inhibitory Mechanisms. Front. Chem 2020, 8, 51. [PubMed: 32117877]

(26). Li Y; Tang H; Zhu H; Kakinen A; Wang D; Andrikopoulos N; Sun Y; Nandakumar A; Kwak E; Davis TP; Leong DT; Ding F; Ke PC Ultrasmall Molybdenum Disulfide Quantum Dots Cage Alzheimer's Amyloid Beta to Restore Membrane Fluidity. ACS Appl. Mater. Interfaces 2021, 13, 29936–29948. [PubMed: 34143617]

(27). Roy R; Paul S HIAPP-Amyloid-Core Derived D -Peptide Prevents HIAPP Aggregation and Destabilizes Its Protofibrils. J. Phys. Chem. B 2022, 126, 822–839. [PubMed: 35060728]

(28). Cummings CG; Hamilton AD Disrupting Protein–Protein Interactions with Non-Peptidic, Small Molecule α-Helix Mimetics. Curr. Opin. Chem. Biol 2010, 14, 341–346. [PubMed: 20430687]

(29). Jayatunga MKP; Thompson S; Hamilton AD α-Helix Mimetics: Outwards and Upwards. Bioorg. Med. Chem. Lett 2014, 24, 717–724. [PubMed: 24433858]

(30). Palanikumar L; Karpauskaite L; Al-Sayegh M; Chehade I; Alam M; Hassan S; Maity D; Ali L; Kalmouni M; Hunashal Y; Ahmed J; Houhou T; Karapetyan S; Falls Z; Samudrala R; Pasricha R; Esposito G; Afzal AJ; Hamilton AD; Kumar S; Magzoub M Protein Mimetic Amyloid Inhibitor Potently Abrogates Cancer-Associated Mutant P53 Aggregation and Restores Tumor Suppressor Function. Nat. Commun 2021, 12, 3962. [PubMed: 34172723]

(31). Davis JM; Tsou LK; Hamilton AD Synthetic Non-Peptide Mimetics of α-Helices. Chem Soc Rev 2007, 36, 326–334. [PubMed: 17264933]

(32). Maity D; Kumar S; AlHussein R; Gremer L; Howarth M; Karpauskaite L; Hoyer W; Magzoub M; Hamilton AD Sub-Stoichiometric Inhibition of IAPP Aggregation: A Peptidomimetic Approach to Anti-Amyloid Agents. RSC Chem. Biol 2020, 1, 225–232. [PubMed: 34458762]

(33). Saraogi I; Hebda JA; Becerril J; Estroff LA; Miranker AD; Hamilton AD Synthetic Alpha-Helix Mimetics as Agonists and Antagonists of Islet Amyloid Polypeptide Aggregation. Angew. Chem. Int. Ed Engl 2010, 49, 736–739. [PubMed: 20029853]

(34). Kumar S; Hamilton AD α-Helix Mimetics as Modulators of Aβ Self-Assembly. J. Am. Chem. Soc 2017, 139, 5744–5755. [PubMed: 28273416]

(35). Maity D; Howarth M; Vogel MC; Magzoub M; Hamilton AD Peptidomimetic-Based Vesicles Inhibit Amyloid-β Fibrillation and Attenuate Cytotoxicity. J. Am. Chem. Soc 2021, 143, 3086–3093. [PubMed: 33600171]

(36). Bunce SJ; Wang Y; Stewart KL; Ashcroft AE; Radford SE; Hall CK; Wilson AJ Molecular Insights into the Surface-Catalyzed Secondary Nucleation of Amyloid-β $_{40}$ (Aβ $_{40}$) by the Peptide Fragment Aβ $_{16–22}$. Sci. Adv 2019, 5, eaav8216. [PubMed: 31245536]

(37). Sun Y; Kakinen A; Wan X; Moriarty N; Hunt CPJ; Li Y; Andrikopoulos N; Nandakumar A; Davis TP; Parish CL; Song Y; Ke PC; Ding F Spontaneous Formation of β-Sheet Nano-Barrels during the Early Aggregation of Alzheimer's Amyloid Beta. Nano Today 2021, 38, 101125. [PubMed: 33936250]

(38). Wiltzius JJW; Sievers SA; Sawaya MR; Cascio D; Popov D; Riekel C; Eisenberg D Atomic Structure of the Cross-β Spine of Islet Amyloid Polypeptide (Amylin). Protein Sci. 2008, 17, 1467–1474. [PubMed: 18556473]

(39). Sun Y; Kakinen A; Zhang C; Yang Y; Faridi A; Davis TP; Cao W; Ke PC; Ding F Amphiphilic Surface Chemistry of Fullerenols Is Necessary for Inhibiting the Amyloid Aggregation of Alpha-Synuclein NACore. Nanoscale 2019, 11, 11933–11945. [PubMed: 31188372]

(40). Sun L; Cho H-J; Sen S; Arango AS; Huynh TT; Huang Y; Bandara N; Rogers BE; Tajkhorshid E; Mirica LM Amphiphilic Distyrylbenzene Derivatives as Potential Therapeutic and Imaging Agents for Soluble and Insoluble Amyloid β Aggregates in Alzheimer's Disease. J. Am. Chem. Soc 2021, 143, 10462–10476 [PubMed: 34213901]

(41). Peng S; Ding F; Urbanc B; Buldyrev SV; Cruz L; Stanley HE; Dokholyan NV Discrete Molecular Dynamics Simulations of Peptide Aggregation. Phys. Rev. E 2004, 69, 041908.

(42). Yin S; Ding F; Dokholyan NV Eris: An Automated Estimator of Protein Stability. Nat. Methods 2007, 4, 466–467. [PubMed: 17538626]

(43). Yin S; Biedermannova L; Vondrasek J; Dokholyan NV MedusaScore: An Accurate Force Field-Based Scoring Function for Virtual Drug Screening. J. Chem. Inf. Model 2008, 48, 1656–1662. [PubMed: 18672869]

(44). Brooks BR; Bruccoleri RE; Olafson BD; States DJ; Swaminathan S; Karplus M CHARMM: A Program for Macromolecular Energy, Minimization, and Dynamics Calculations. J. Comput. Chem 1983, 4, 187–217.

(45). Lazaridis T Effective Energy Functions for Protein Structure Prediction. Curr. Opin. Struct. Biol 2000, 10, 139–145. [PubMed: 10753811]

(46). Ding F; Borreguero JM; Buldyrey SV; Stanley HE; Dokholyan NV Mechanism for the α-Helix to β-Hairpin Transition. Proteins Struct. Funct. Genet 2003, 53, 220–228. [PubMed: 14517973]

(47). Nedumpully-Govindan P; Jemec DB; Ding F CSAR Benchmark of Flexible MedusaDock in Affinity Prediction and Nativelike Binding Pose Selection. J. Chem. Inf. Model 2016, 56, 1042–1052. [PubMed: 26252196]

(48). Ding F; Dokholyan NV Emergence of Protein Fold Families through Rational Design. PLoS Comput. Biol 2006, 2, e85. [PubMed: 16839198]

(49). Proctor EA; Yin S; Tropsha A; Dokholyan NV Discrete Molecular Dynamics Distinguishes Nativelike Binding Poses from Decoys in Difficult Targets. Biophys. J 2012, 102, 144–151. [PubMed: 22225808]

(50). Nedumpully-Govindan P; Kakinen A; Pilkington EH; Davis TP; Chun Ke P; Ding F Stabilizing Off-Pathway Oligomers by Polyphenol Nanoassemblies for IAPP Aggregation Inhibition. Sci. Rep 2016, 6, 19463. [PubMed: 26763863]

(51). Kakinen A; Adamcik J; Wang B; Ge X; Mezzenga R; Davis TP; Ding F; Ke PC Nanoscale Inhibition of Polymorphic and Ambidextrous IAPP Amyloid Aggregation with Small Molecules. Nano Res. 2018, 11, 3636–3647. [PubMed: 30275931]

(52). Srinivasan E; Rajasekaran R Molecular Binding Response of Naringin and Naringenin to H46R Mutant SOD1 Protein in Combating Protein Aggregation Using Density Functional Theory and Discrete Molecular Dynamics. Prog. Biophys. Mol. Biol 2019, 145, 40–51. [PubMed: 30543828]

(53). Hanwell MD; Curtis DE; Lonie DC; Vandermeersch T; Zurek E; Hutchison GR Avogadro: An Advanced Semantic Chemical Editor, Visualization, and Analysis Platform. J. Cheminformatics 2012, 4, 17.

(54). Kabsch W; Sander C Dictionary of Protein Secondary Structure: Pattern Recognition of Hydrogen-Bonded and Geometrical Features. Biopolymers 1983, 22, 2577–2637. [PubMed: 6667333]

(55). Rodriguez Camargo DC; Tripsianes K; Buday K; Franko A; Göbl C; Hartlmüller C; Sarkar R; Aichler M; Mettenleiter G; Schulz M; Böddrich A; Erck C; Martens H; Walch AK; Madl T; Wanker EE; Conrad M; de Angelis MH; Reif B The Redox Environment Triggers Conformational Changes and Aggregation of HIAPP in Type II Diabetes. Sci. Rep 2017, 7, 44041. [PubMed: 28287098]

(56). Maj M; Lomont JP; Rich KL; Alperstein AM; Zanni MT Site-Specific Detection of Protein Secondary Structure Using 2D IR Dihedral Indexing: A Proposed Assembly Mechanism of Oligomeric HIAPP. Chem. Sci 2018, 9, 463–474. [PubMed: 29619202]

(57). Sun Y; Kakinen A; Xing Y; Pilkington EH; Davis TP; Ke PC; Ding F Nucleation of β-Rich Oligomers and β-Barrels in the Early Aggregation of Human Islet Amyloid Polypeptide. Biochim. Biophys. Acta BBA - Mol. Basis Dis 2019, 1865, 434–444.

(58). Zhang Y; Liu Y; Tang Y; Zhang D; He H; Wu J; Zheng J Antimicrobial α-Defensins as Multi-Target Inhibitors against Amyloid Formation and Microbial Infection. Chem. Sci 2021, 12, 9124–9139 [PubMed: 34276942]

(59). Cohlberg JA; Li J; Uversky VN; Fink AL Heparin and Other Glycosaminoglycans Stimulate the Formation of Amyloid Fibrils from α-Synuclein in Vitro. Biochemistry 2002, 41, 1502–1511. [PubMed: 11814343]

(60). Relini A; De Stefano S; Torrassa S; Cavalleri O; Rolandi R; Gliozzi A; Giorgetti S; Raimondi S; Marchese L; Verga L; Rossi A; Stoppini M; Bellotti V Heparin Strongly Enhances the Formation of B2-Microglobulin Amyloid Fibrils in the Presence of Type I Collagen. J. Biol. Chem 2008, 283, 4912–4920. [PubMed: 18056266]

(61). Potter KJ; Werner I; Denroche HC; Montane J; Plesner A; Chen Y; Lei D; Soukhatcheva G; Warnock GL; Oberholzer J; Fraser PE; Verchere CB Amyloid Formation in Human Islets Is Enhanced by Heparin and Inhibited by Heparinase: Heparin Stimulates Islet Amyloid Formation. Am. J. Transplant 2015, 15, 1519–1530. [PubMed: 25833002]

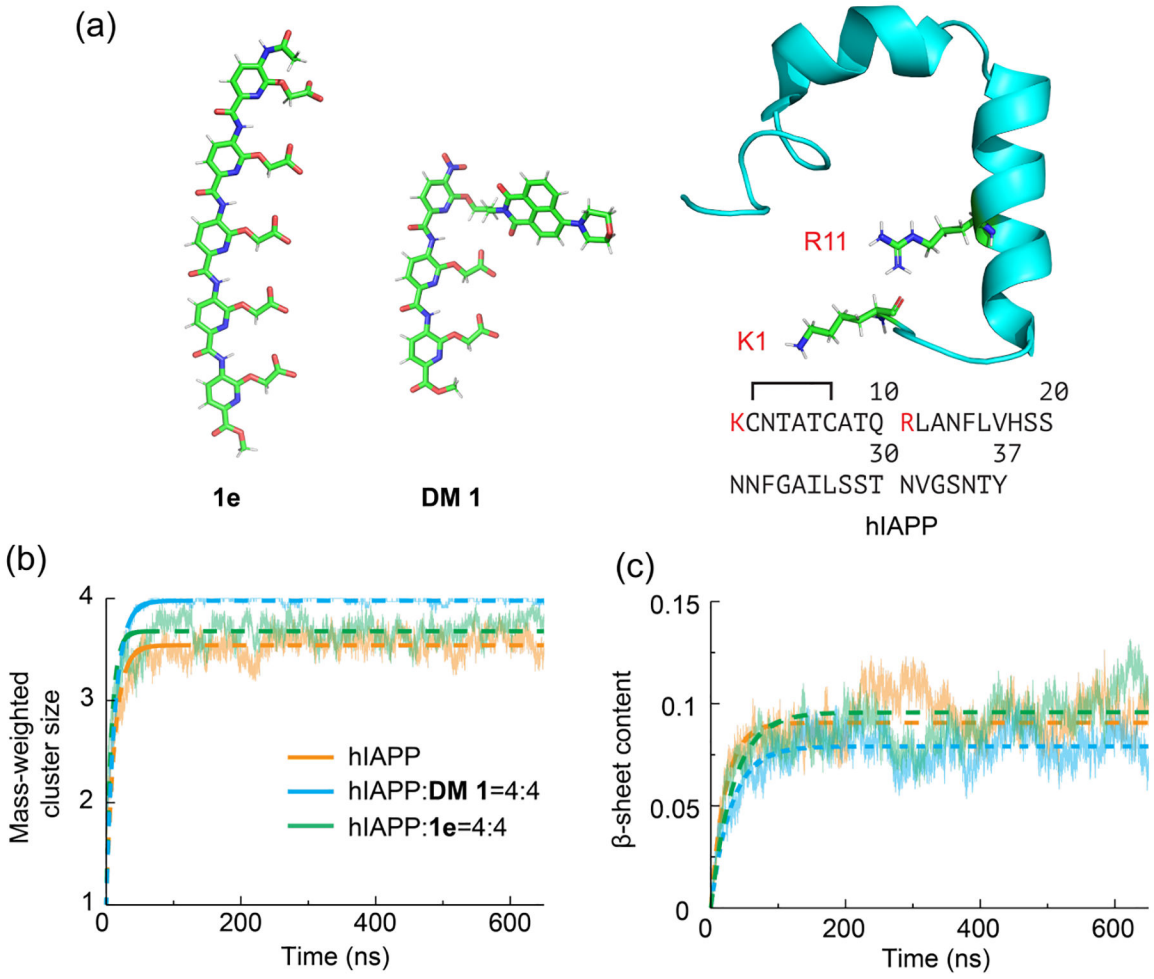

Figure 1. Kinetics of hIAPP aggregation in the absence and presence of helix mimetics.

(A) Structure illustrations of **1e** (left panel), **DM 1** (middle panel) and hIAPP monomer (right panel). Helix mimetics **1e** and **DM 1** were shown as sticks and hIAPP (PDB ID: 2L86) was shown as carton with the residues K1 and R11 highlighted as sticks. The carbon, nitrogen, oxygen and hydrogen elements were colored in green, blue, red and gray, respectively. The amino acid sequence of hIAPP was shown with the positive charged residues colored in red and disulfide bond indicated by black line. (B) Mass-weighted cluster size of hIAPP peptides as a function of time was obtained by averaging over independent simulations in the absence and presence of **1e** and **DM 1**. The dashed lines showed the kinetics fitted with $y=M(1-\exp(-t/T))+1$, where M and T were fitting parameters. (C) β-sheet content of hIAPP peptides as a function of time in the absence and presence of **1e** and **DM 1**. The dashed lines showed the kinetics fitted with $y=A(1-\exp(-t/\tau))$, where A and τ were fitting parameters.

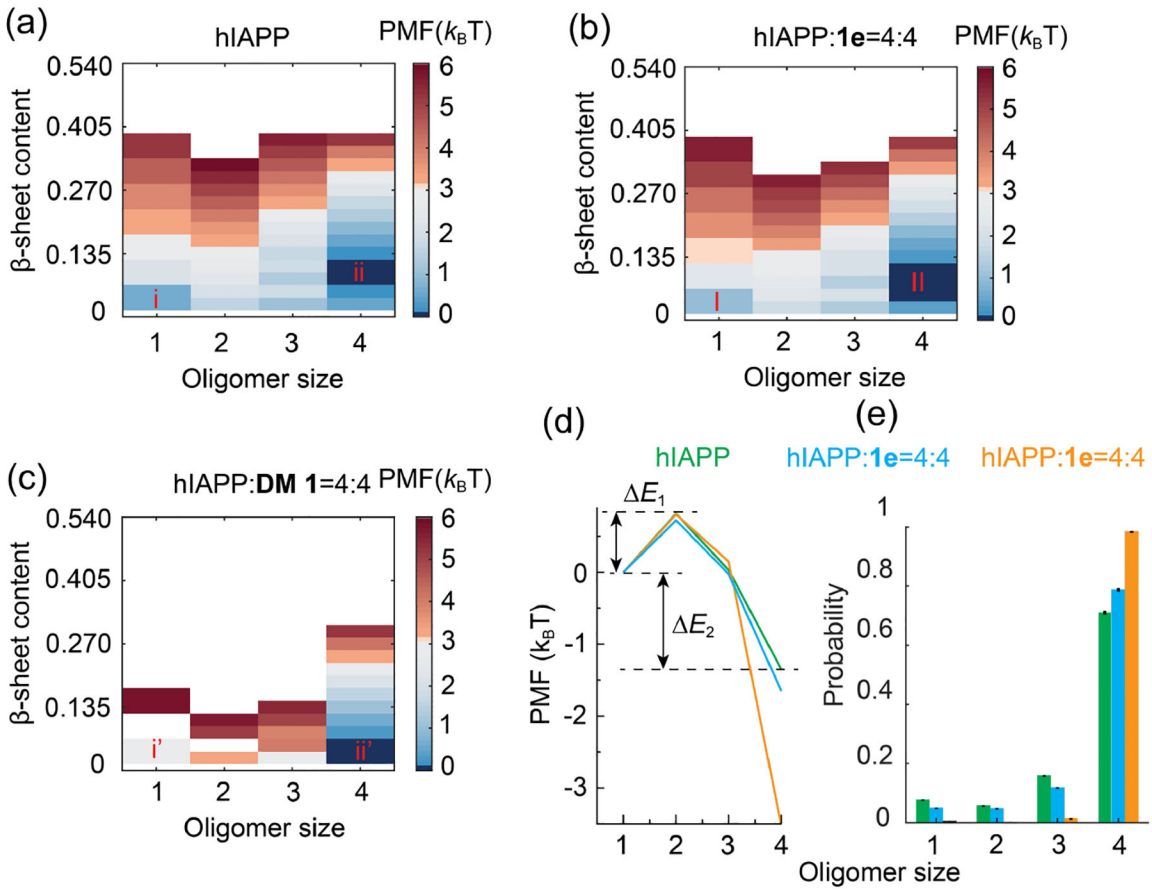

Figure 2. Aggregation free energy landscape of hIAPP in the absence and presence of helix mimetics.

Two-dimensional PMF with respect to the oligomer size and β-sheet content for (A) hIAPP peptides and in the presence of (B) **1e** and (C) **DM 1**. (D) One-dimensional PMF with respect to the oligomer size. (E) Probability distribution of the oligomer size formed in the presence and absence of **1e** and **DM 1**.

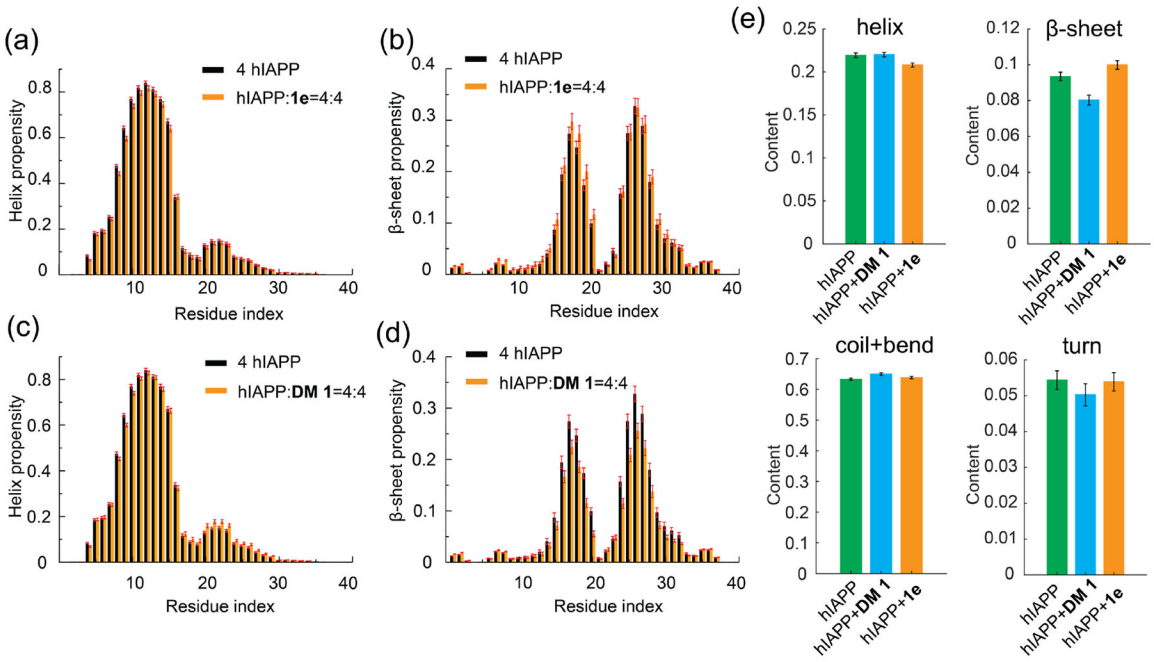

Figure 3. Secondary structure of hIAPP in the presence of helix mimetics.

Secondary structure propensities of each hIAPP residue in the presence of (A, B) **1e** and (C, D) **DM 1**. (A, C) helical structure; (B, D) β-sheet structure. (E) Overall secondary structure contents of hIAPP peptides in the absence and presence of **1e** and **DM 1**. Data were shown as mean ± SEM of 39 independent simulations.

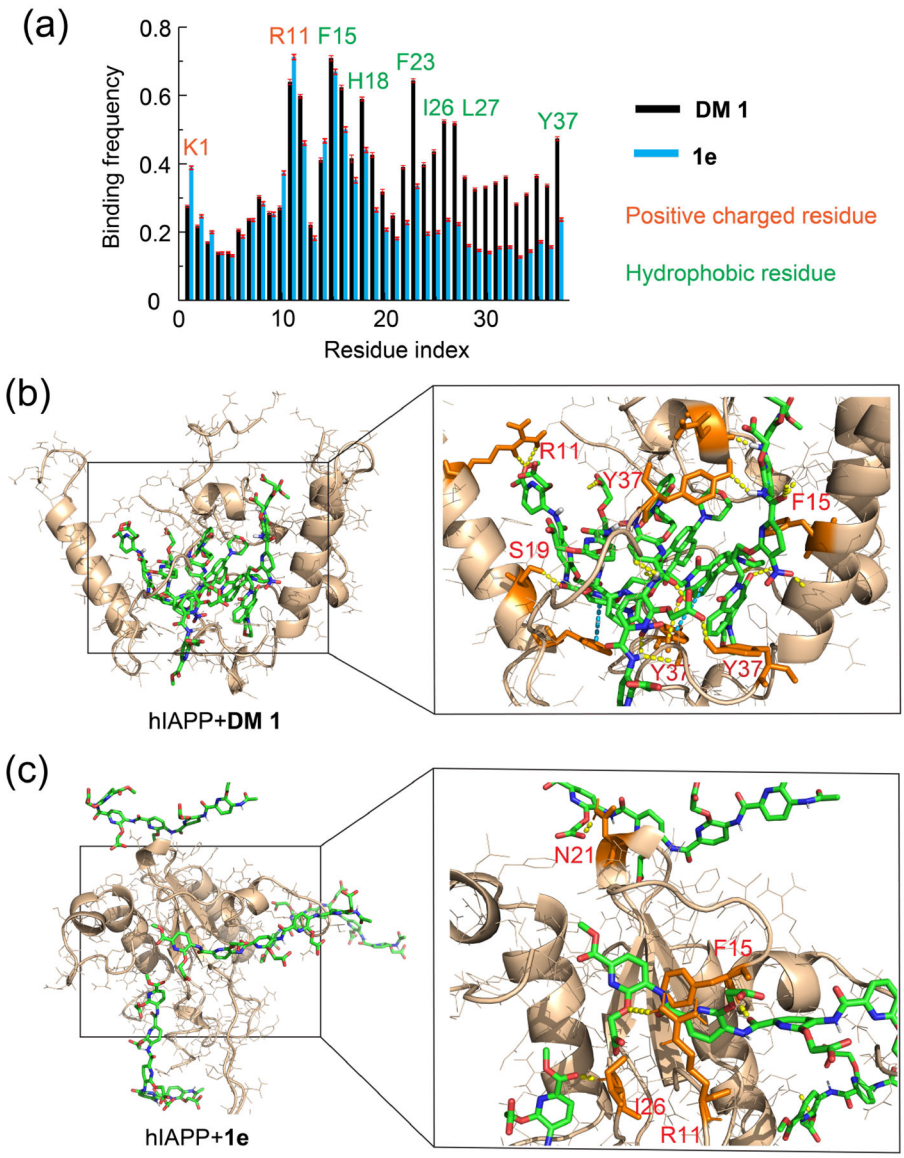

Figure 4. Binding behaviors of helix mimetics with hIAPP peptides.

(A) Binding frequency of **DM 1** and **1e** with each residue of hIAPP peptides. Residues with peak binding frequencies were highlighted and labeled. Data were shown as mean values ± SEM of 39 independent simulations. (B, C) *Left panels:* Typical binding conformation of hIAPP with (B) **DM 1** and (C) **1e**. hIAPP peptides were shown as wheat cartons and lines, whereas the helix mimetics were shown as sticks colored by elements. *Right panels:* Zoomed-in snapshots of the boxed region in the left panels. Polar interactions and π-π stackings were respectively showed in yellow and cyan dashed lines. Binding residues were highlighted as orange sticks.

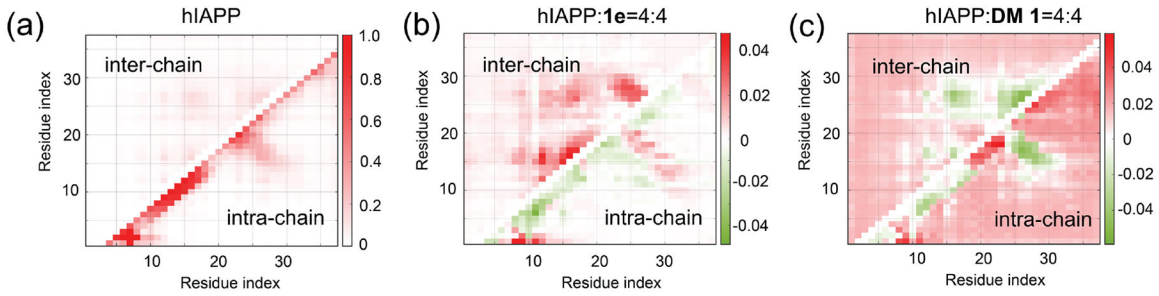

Figure 5. Residue-wise inter- and intra-peptide contact frequency maps of hIAPP peptides.

(A) Contact frequency maps of hIAPP tetramer. (B, C) Changes of contact frequency maps in the presence of (B) **1e** and (C) **DM 1** with respect to the hIAPP tetramer.

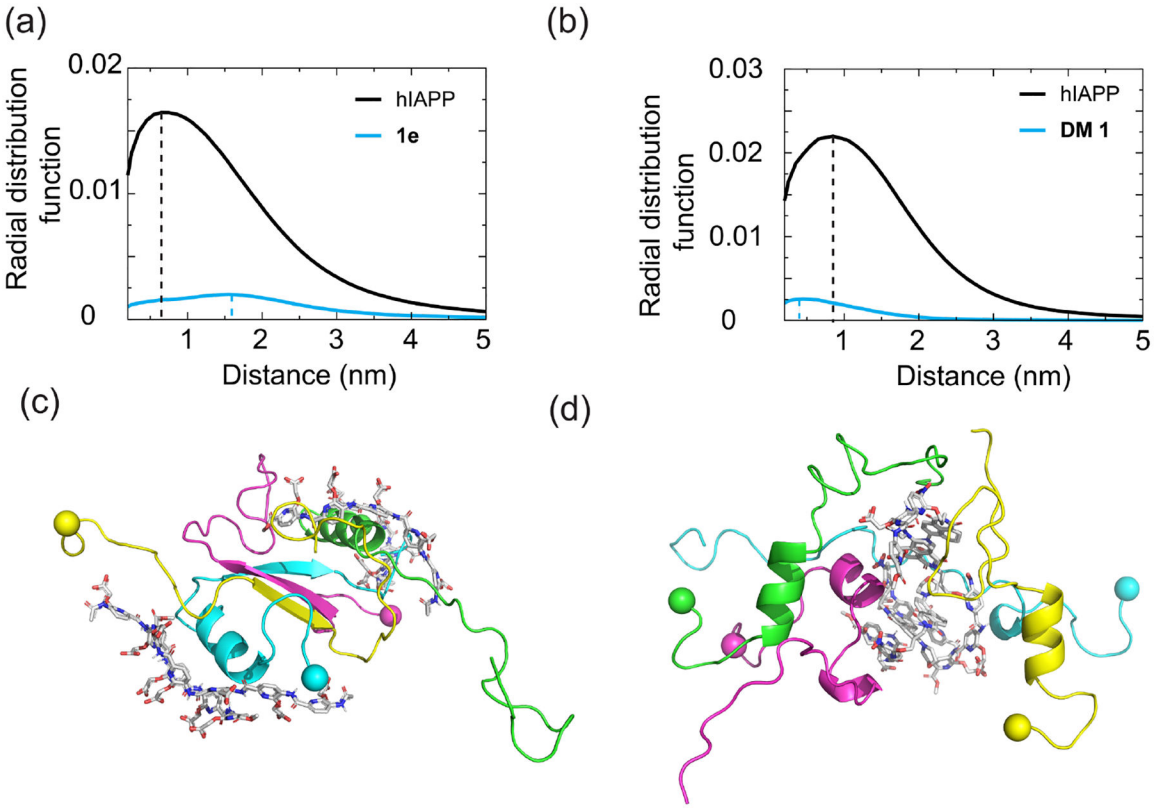

Figure 6. Three-dimensional structural properties of hIAPP-DM 1 and hIAPP-1e complexes.

(A, B) Radial distribution functions of hIAPP and helix mimetics atoms from the center of mass of the cluster. (A) hIAPP and **1e**. (B) hIAPP and **DM 1**; Peaks were indicated by dashed lines. Typical conformations of systems with (C) hIAPP:**1e**=4:4 and (D) hIAPP:**DM 1**=4:4. hIAPP peptides were shown as cartons with N-termini indicated by spheres and helix mimetics were shown as sticks.

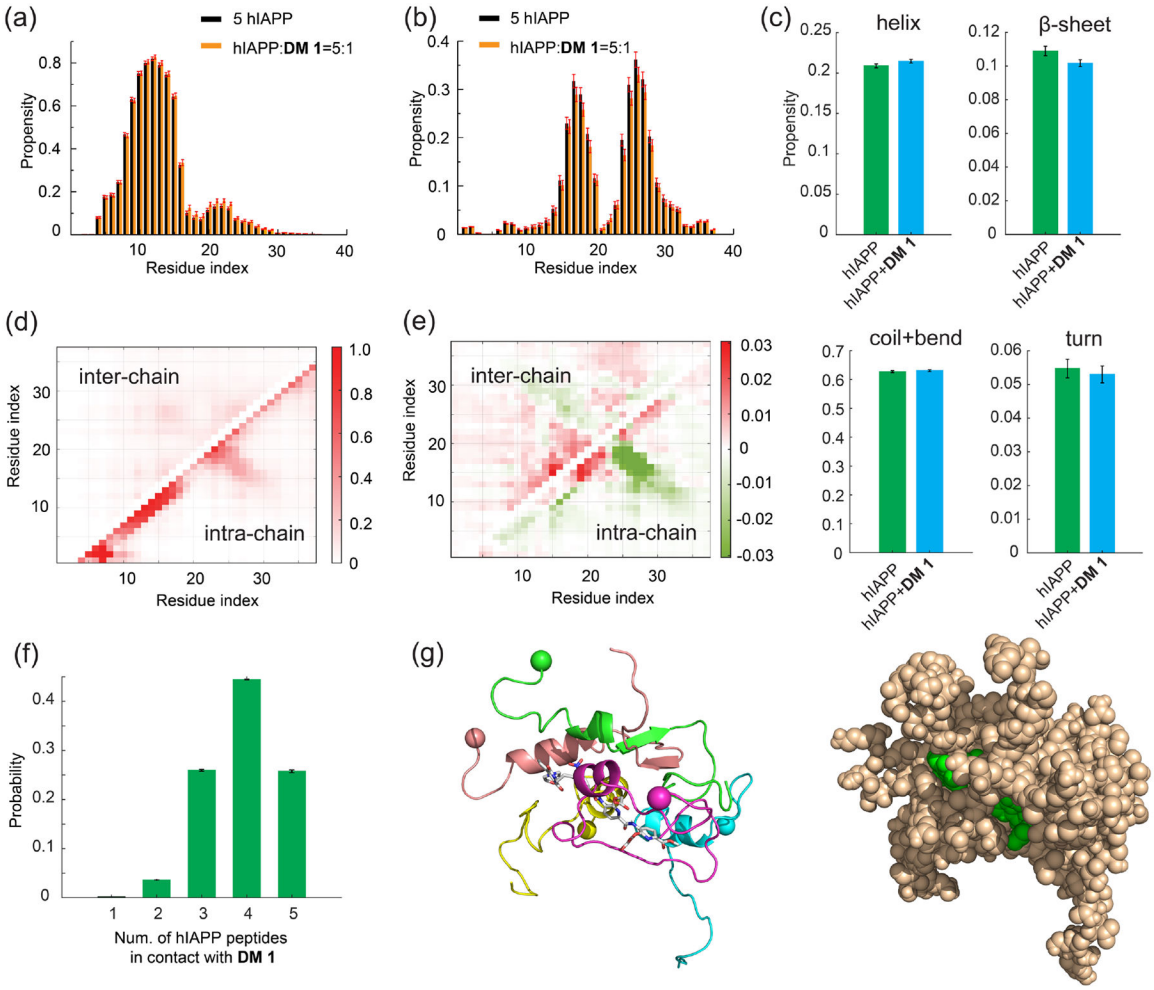

Figure 7. Interactions between hIAPP and DM 1 at substoichiometric concentration ratio hIAPP:DM 1=5:1.

(A) Helix and (B) β-sheet structure propensities of each hIAPP. (C) Overall secondary structure contents of hIAPP peptides in the absence and presence of **DM 1**. (D) Contact frequency maps of hIAPP pentamer. (E) Changes of contact frequency maps in the presence of **DM 1** compared to the hIAPP pentamer. (F) Probability distribution of the number of hIAPP peptides in contact with **DM 1**. (G) Typical snapshoots of hIAPP-**DM 1** complex at concentration ratio hIAPP:**DM 1**=5:1. *Left panel*: hIAPP peptides shown as cartons and helix mimetics shown as sticks. *Right panel:* hIAPP peptides shown as wheat spheres and helix mimetics shown as green spheres.